ELSEVIER

Computational Materials Science 24 (2002) 490–500

COMPUTATIONAL MATERIALS SCIENCE

www.elsevier.com/locate/commatsci

Simulation of time-discontinuous chemically-aided intergranular fracture

T.I. Zohdi *

Department of Mechanical Engineering, The University of California at Berkeley, 6195 Etcheverry Hall, Berkeley, CA 94720-1740, USA

Received 28 September 2001; received in revised form 17 December 2001; accepted 18 December 2001

Abstract

In this work, based on experimental observations, a model for the pressure dependent diffusion and accumulation of hydrogen ahead of a propagating intergranular crack front is developed. In the model, the pressure dependency of the diffusion is incorporated into the activation energy of an Arrhenius form of the material's diffusivity tensor along high-diffusivity grain boundaries. Inherent to the model is that large amounts of hydrogen can be absorbed into the crack's process zone, due to the high triaxial stress in that region, which produces a larger effective diffusivity locally. Further ahead, the effective diffusivity quickly decreases. The combined effect forms a barrier to further rapid penetration, which leads to the mentioned accumulation of the hydrogen in the process zone. Theoretical aspects of the model are discussed and numerical simulations of the transient distributions of hydrogen and subsequent crack front propagation are performed to illustrate the main characteristics of the model.

Keywords: Fracture; Intergranular; Hydrogen

1. Introduction

In a large number of cases, environmentally induced intergranular cracking mechanisms have at their root the absorption or internal production of hydrogen. Due to its relatively small atomic size, hydrogen easily penetrates most solid materials. In metals, a common penetration mechanism is by hydrogen traveling down high diffusivity grain boundaries (Fig. 1). Experimentally, it is frequently observed that hydrogen accumulates in locations of high positive triaxial stress. In a sense, one can interpret the microstructure as becoming "opened up", and thus providing more energetically favorable places for diffusion. Further details and thermodynamically-based arguments related to pressure dependency of the diffusivity can be found in Flynn [13]. There are a variety of possible associated hydrogen damage mechanisms. See Fontana [14] or the Metals Handbook [15] for case studies. In general, the relatively high energy states of stressed materials lowers the barrier to ionization (stripping off of electrons). Most physical systems attempt to equilibrate the ionic concentration, which can lead to detrimental metallurgical changes, as well as production of high pressure gas. Grain boundaries are such high energy regions, and are therefore highly susceptible to accelerated

* Tel.: +1-510-642-6834; fax: +1-510-642-9172.
E-mail address: zohdi@newton.berkeley.edu (T.I. Zohdi).

0927-0256/02/$ - see front matter
PII: S0927-0256(02)00155-6

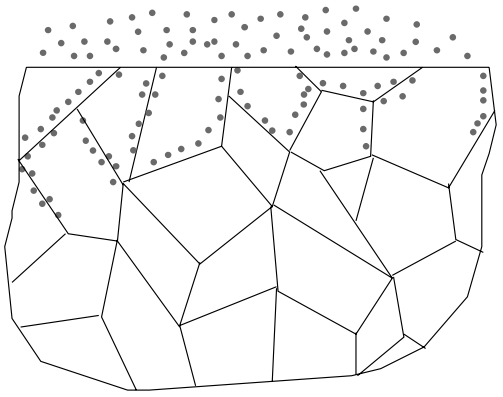

Fig. 1. Hydrogen absorption into the interior of a solid via grain boundary diffusion.

attack in an aggressive environment. The end effect of the chemical reactions at the grain boundaries is that cleavage fractures occur. There a number of other possible variants and combinations of the mentioned grain boundary degradation mechanisms. For example, there are a variety of models which attempt to describe the processes that take place in the process zone that lead to subcritical fracture, such as hydride inclusion formation and hydrogen enhanced localized plasticity (HELP), as advocated by Birnbaum and collaborators. Clearly, no single model can completely explain all hydrogen damage. However, common to these modes of hydrogen failure is the fact that the grain boundaries rupture, and that this failure is directly related to the presence of hydrogen. We refer the reader to [1,4–7,10–12,16–35]. The preceding models concentrate on a different aspect of chemically-aided fracture, essentially on (smaller scale) mechanisms within the process zone leading to subcritical crack progression. In this work, a fairly general computational model is developed, which can be used in conjunction with the majority of referenced models.

1.1. A specific case of interest: experimental observations

In Zohdi and Meletis [35] time-discontinuous hydrogen-assisted mode-I intergranular cracking was observed in rolled aluminum–lithium alloy in the T6 condition (2090 AL–2.2Li–2.9Cu–0.12Zr). The term *time-discontinuous* denotes that the crack front propagated, then arrested, with the process then repeating itself. In other words, *crack fronts grew discontinuously with time*, i.e. they appeared to "jump". In the mentioned laboratory experiments, the material was produced in the form of a rolled plate, and its microstructure consisted of flattened grains with average dimensions of 1100 μm × 240 μm × 11 μm. Double cantilevered beam (DCB) specimens were prepared from the plate in such a way that the crack plane was parallel to the flattened grain boundaries. The DCB specimens were 2.54 cm high (plate thickness), 1.3 cm wide and 12.5 cm long, providing valid plane strain conditions in the specimen interior. The specimen was first fatigue precracked to develop a sharp and straight crack front. The specimen was then subsequently tested in a 3.5% NaCl solution (pH = 6.9) under cathodic charging to induce hydrogen adsorption on the crack root and was loaded at a constant $K_I = 8.62$ MPa $\sqrt{\text{m}}$. The crack growth measurements showed that a crack front advances in a discontinuous manner, with a relatively consistent overall crack velocity of approximately 5×10^{-8} m/s. Scanning electron microscope (SEM) examinations of the fracture surfaces showed an exclusively intergranular cracking mode. Detailed fracture surface observations revealed the presence of two types of crack-arrest markings (CAM); micro- and macro-CAM. The micro-CAM indicated that the position of the individual crack jumps, and their average spacing was approximately between 20 and 30 μm. Both types of CAM ran perpendicular to the direction of the crack propagation. Measurements of the spacing between macro-CAM showed that they corresponded to the jump events monitored on the specimen surface. Therefore, the measured velocity reflects the overall crack velocity relates to the time to ligament fracture, and *not to the individual jump times*, which are relatively short. In other words, the intergranular crack front "paused" at these locations (macro-CAM) until the ligaments were fractured by stress-chemical interaction. The measured incremental amount of crack front advance corresponded quite well to the process zone size ahead of the crack, which was also estimated to be between 20 and 30 μm. Due to

the micro-CAM markings, the experiments suggested that some type of microfissuring occurred in the vicinity of the process zone boundary which propagates backwards and connects to the intergranular crack front. In summary, the incremental ligament fracture ahead of the crack appears to be the slowest step and controls the overall crack velocity. The experiments suggest that for the crack front to advance, "incubation time" is needed to sufficiently degrade the material in the hydrogen saturated process zone.

1.2. Scope of the work

The goal of this work is to develop a relatively *simple* model to simulate the described series of events. The outline of the paper is as follows. In Section 2, a model to simulate the pressure dependent diffusion and accumulation of hydrogen ahead of a intergranular crack front is developed. In Section 3, an approximation to the pressure field is discussed. In Section 4, a computational procedure is presented for the propagation of a crack front. In Section 5, numerical experiments are conducted and the results are discussed. In Section 6, some concluding comments are given.

2. Pressure-dependent diffusion models

The mass balance for a small diffusing species, denoted by the normalized concentration of the solute c (molecules per unit volume), in an arbitrary subvolume of material contained within Ω, denoted ω, consists of a storage term ($\dot{c}$) and an inward normal flux term ($-\boldsymbol{G}\cdot\boldsymbol{n}$), leading to $\int_\omega \dot{c}\,\mathrm{d}\omega = -\int_{\partial\omega} \boldsymbol{G}\cdot\boldsymbol{n}\,\mathrm{d}a$. After using the divergence theorem, since the volume ω is arbitrary, one has

$$\dot{c} = \nabla\cdot(\mathbb{D}_0 \mathrm{e}^{-U/R\theta}\cdot\nabla c), \tag{1}$$

where the familiar Arrhenius form has been used, where $\mathbb{D}_0$ is the diffusivity tensor (area per unit time) at a reference temperature, U is the activation energy for solute motion per mole of diffusive species, R is the universal gas constant and θ is the temperature. Clearly, on the micro-continuum scale, the diffusivity tensor of the material is a phenomenological parameter, which depends on the temperature. However, additionally it is also sometimes observed that, in regions of relatively high positive triaxial stress, the diffusion is accelerated, while in regions of high negative triaxial stress, diffusion is decelerated.

A simple constitutive model to incorporate stress-dependency phenomena is given by a pseudo-Fickian/Arrhenius law, $\boldsymbol{G} = -\mathbb{D}_0 \mathrm{e}^{-U(\boldsymbol{\sigma})/R\theta}\cdot\nabla c$. An additive split for stress dependency can be written as [36] $U(\boldsymbol{\sigma}) = U_0 + \widetilde{U}(P)$, where U_0 is a stress-independent reference activation energy and $P = -\mathrm{tr}\,\boldsymbol{\sigma}/3$ is the pressure. Such a split can be motivated by thermodynamical arguments found in Flynn [13]. It is logical to require that the function $\widetilde{U}(P)$ have the following properties:

$$\begin{aligned} &\widetilde{U}(P) < 0 \quad \text{for } P < 0,\\ &\widetilde{U}(P) > 0 \quad \text{for } P > 0,\\ &\widetilde{U}(P) = 0 \quad \text{for } P = 0. \end{aligned} \tag{2}$$

If we expand $\widetilde{U}(P)$ around $P = 0$ we have

$$\widetilde{U}(P) = 0 + \frac{\partial \widetilde{U}(P)}{\partial P|_{P=0}} P + \cdots = \eta P = -\eta\frac{\mathrm{tr}\,\boldsymbol{\sigma}}{3}, \quad \eta \geqslant 0.$$

Therefore we have $U \approx U_0 - \eta(\mathrm{tr}\,\boldsymbol{\sigma}/3)$. The parameter can be considered as an "activation volume", and is discussed at length in Flynn [13]. Therein, experimental results are tabulated for various solid/solute combinations. Essentially, the embedding of a spatially-variable pressure field into a spatially-constant diffusivity, transforms the diffusivity into a spatially heterogeneous diffusivity. Thus, the solid appears to have a heterogeneous diffusive composition of relatively high diffusivity in negative pressure regions and relatively low diffusivity in positive pressure regions.

3. Approximate pressure fields

To model the pressure fields ahead of the crack front, we consider an initially sharp mode-I crack, producing a singular linearly-elastic stress field, where $\sigma_{ij} = (K_\mathrm{I}/\sqrt{2\pi r}) f_{ij}(\phi)$ and where the f_{ij} are functions of ϕ (Fig. 2). Using standard notation, the stress intensity factor is $K_\mathrm{I} = \zeta\sigma\sqrt{a}$, where a is half the length of the crack and where σ is the remote stress. For an infinite planar domain

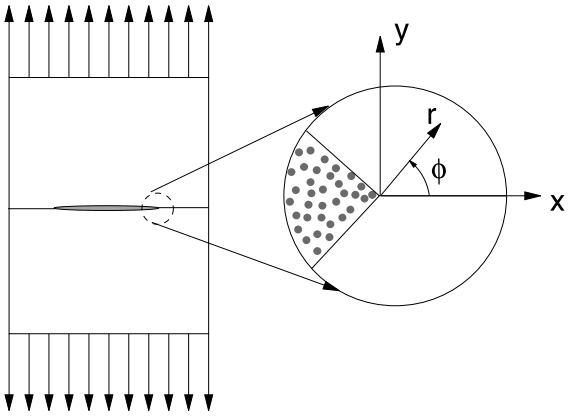

Fig. 2. An idealization of an intergranular crack front with hydrogen adsorbed onto the root of the crack tip.

under remote uniaxial loading we have $\zeta = \sqrt{\pi}$. Throughout the analysis we consider only plane strain conditions. Correspondingly, we have

$$\begin{aligned}
\sigma_{xx} &= \frac{K_{\mathrm{I}}}{\sqrt{2\pi r}} \cos\frac{\phi}{2}\left(1 - \sin\frac{\phi}{2}\sin\frac{3\phi}{2}\right),\\
\sigma_{yy} &= \frac{K_{\mathrm{I}}}{\sqrt{2\pi r}} \cos\frac{\phi}{2}\left(1 + \sin\frac{\phi}{2}\sin\frac{3\phi}{2}\right),\\
\sigma_{xy} &= \frac{K_{\mathrm{I}}}{\sqrt{2\pi r}} \sin\frac{\phi}{2}\cos\frac{\phi}{2}\cos\frac{3\phi}{2},\\
\sigma_{xz} &= \sigma_{yz} = 0, \quad \sigma_{zz} = v(\sigma_{xx} + \sigma_{yy}),
\end{aligned} \tag{3}$$

and therefore, for the pressure

$$P(r,\phi) = -\frac{2(1+v)}{3}\frac{K_{\mathrm{I}}}{\sqrt{2\pi r}}\cos\frac{\phi}{2}, \tag{4}$$

where v is the material Poisson ratio. At the crack tip, the pressure is singular ($P = \mathcal{O}(r^{-1/2})$), and thus when inserted into the Arrhenius law, the diffusivity also becomes singular, if the material remains linearly elastic. However, we consider that material and geometric nonlinearities occur (such as crack blunting) in the process zone and thus the stresses at the tip remain finite. An approximation of the nonlinear pressure field is determined by first computing the domain within an envelope of points where the von Mises criteria holds, i.e. $\boldsymbol{\sigma}'$: $\boldsymbol{\sigma}' = 2\mathscr{Y}^2/3$, where $\boldsymbol{\sigma}'$ is the deviatoric stress, and $\mathscr{Y}$ is the yield stress obtained from a uniaxial tension test. Under plane strain conditions, this leads to a radial envelope function of the process zone given by

$$r_p(\phi) = \frac{K_{\mathrm{I}}^2}{4\pi\mathscr{Y}^2}\left(\frac{3}{2}\sin^2\phi + (1-2v)^2(1+\cos\phi)\right). \tag{5}$$

Specifically at $\phi = 0$, we have the well known relation $r_p = (K_{\mathrm{I}}^2/2\pi\mathscr{Y}^2)(1-2v)^2$. Since the diffusion along grain boundaries is approximately 1000 times greater than in the transgranular direction, for the materials of interest in this work, the diffusion process is considered to be one-dimensional. Therefore, a specific plane, that of $\phi = 0$, i.e. along the grain boundary, is of primary importance. The pressure is approximated as being constant throughout the process zone, given by the elastic value at $x = r_p$ and $\phi = 0$

$$P^* \stackrel{\mathrm{def}}{=} P(x = r_p, \phi = 0) = -\frac{2(1+v)}{3}\frac{K_{\mathrm{I}}}{\sqrt{2\pi r_p}}. \tag{6}$$

This pressure is used in the process zone, while the elastic solution field is used in the remainder of the body. The approximations neglect the redistribution of the stress field in the elastic portion of the body, and are thus accurate only when the process zone size is small compared to other length scales in the problem. This is assumed to be the case in the present study. We remark that the process zone size (along the $\phi = 0$ plane) tends to zero as the incompressible limit is approached, and thus the average pressure in the process zone becomes infinite. The Poisson ratio of the aluminum–lithium alloy used in this work was approximately $v = 0.295$, which produces process zone (small) sizes safely within the range of validity of the assumptions made in the derivation of the expressions.

4. Intergranular crack front growth

We assume that $\mathbb{D} = \mathbb{D}_0 \mathrm{e}^{-U(\boldsymbol{\sigma})/R\theta}$ is isotropic, but spatially variable (due to the variation of the pressure). Therefore, $\mathbb{D}_0$ can be represented by $\mathbb{D}_0 = D_0\boldsymbol{I}$ in three dimensions and simply a scalar function D_0 in one dimension. In order to extract some qualitative information on the behavior of the model, we first consider a two point boundary value problem describing *steady state* diffusive solution behavior along a grain boundary. Accordingly, consider a ligament ahead of a mode-I

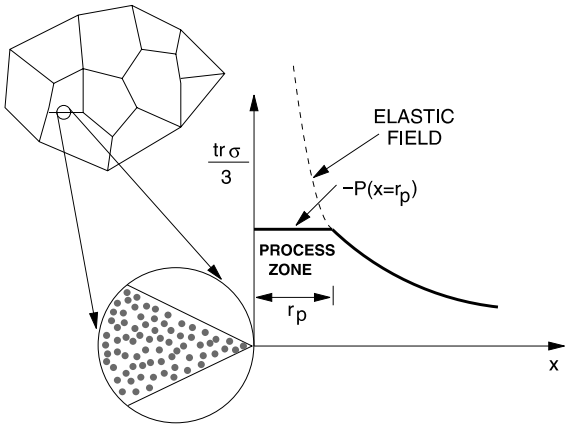

Fig. 3. An approximation of the pressure in the process zone.

crack (Fig. 3) to form the following two point boundary value problem: $\nabla \cdot (D_0 \mathrm{e}^{-U(\boldsymbol{\sigma})/R\theta} \cdot \nabla c) = \dot{c} = 0, \quad c(x=0,t) = c_s = 1 \quad \text{and} \quad c(x=L,t) = 0.$ The solution is monotonically decreasing, starting from the front surface

$$c(x) = c_s + M \int_0^x \frac{1}{D_0 \mathrm{e}^{-(U_0+\eta P)/R\theta}}\,\mathrm{d}x, \quad \text{where } M = -\frac{c_s}{\int_0^L \frac{1}{D_0 \mathrm{e}^{-(U_0+\eta P)/R\theta}}\,\mathrm{d}x}. \tag{7}$$

Since the term $D_0 \mathrm{e}^{-(U_0+\eta P)/R\theta}$ is relatively large in the process zone, the concentration stays relatively high in that region. However, once $D_0 \mathrm{e}^{-(U_0+\eta P)/R\theta}$ starts to drop, the concentration decreases more rapidly. Essentially, a "flux-barrier" is formed that permits only limited solute penetration, i.e. low concentration gradients and low fluxes. The pressure field ahead of the crack will lead high solute accumulation, since the homogeneous diffusivity (D_0) is transformed into a spatially heterogeneous one ($D_0 \mathrm{e}^{-(U_0+\eta P)/R\theta}$). The concentration gradient is

$$\frac{\mathrm{d}c(x)}{\mathrm{d}x} = \frac{M}{D_0} \mathrm{e}^{(U_0+\eta P)/R\theta},$$

thus one observes that the term controlling the concentration gradient is $\mathrm{e}^{(U_0+\eta P)/R\theta}$ drops rapidly, thus locally trapping the hydrogen. One can interpret the stress state as producing a relatively high effective diffusivity immediately ahead of the crack. Outside the process zone the effective diffusivity then decreases rapidly. The combined effects cause accumulation of hydrogen in the process zone. For the transient distributions, if the diffusivity were to remain constant, the boundary value problem could be solved analytically. However, because of the pressure induced heterogeneous effective diffusivity, the boundary value problem must be solved numerically. We employ an implicit finite difference scheme to compute the diffusion of the hydrogen.

4.1. Numerical discretization

For the mentioned reasons (highly diffusive grain boundaries), we consider only the one-dimensional case, i.e. diffusion along the grain boundaries. Using a central finite difference stencil for the representation of the flux we have

$$D\frac{\mathrm{d}c}{\mathrm{d}x} \approx D(x)\frac{c(x+h)-c(x-h)}{2h},$$

where h is the uniform grid spacing for the x direction. Applying the difference formula once again to the flux, we obtain

$$\frac{\mathrm{d}}{\mathrm{d}x}\left(D\frac{\mathrm{d}c}{\mathrm{d}x}\right) = \underbrace{\frac{D(x+h)c(x+2h) - (D(x-h)+D(x+h))c(x) + D(x-h)c(x-2h)}{4h^2}}_{\stackrel{\text{def}}{=}\lambda(c)}. \tag{8}$$

The time dependent term is also approximated by a difference approximation at t, $\dot{c} \approx (c|_{t+\delta t} - c|_t)/\delta t$. The standard scheme is as follows for $0 \leqslant \Lambda \leqslant 1$:

$$\underbrace{\Lambda\lambda(c)}_{\text{evaluated at } t} + \underbrace{(1-\Lambda)\lambda(c)}_{\text{evaluated at } t+\delta t} = \underbrace{\dot{c}}_{\text{evaluated at } t+\delta t}. \tag{9}$$

If $\Lambda = 1$ we have the implicit "backward Euler" approximation, while if $\Lambda = 0$ we have the explicit "forward Euler" approximation. In the computational experiments to follow later, we have used an

implicit midpoint rule of $\Lambda = 0.5$, thus requiring a system of equations to be solved at each time step. We used a standard frontal successive over relaxation (SOR) iteration procedure to solve the system of equations, which, for the sake of completeness, is discussed next.

4.2. An iterative frontal SOR algebraic system solver

Since we will later introduce reactions into the analysis, we discuss the numerical solution scheme for the one-dimensional analog to the more general reaction-diffusion equation, $\dot{c} = \nabla \cdot (\mathbb{D} \cdot \nabla c) - \tau c$. Within a time step, we used the SOR method to solve the algebraic system of equations. Following the standard procedure, we group together terms and apply the SOR iteration procedure in a moving front fashion. *We emphasize that this "solution front" is not the crack front*. The usual procedure is to first perform a Gauss–Seidel iteration, then to accelerate the solution with an SOR update. All nodes behind the solution front, i.e. behind the node in question, have the updated SOR values, while those ahead have the previous iteration values. We have four terms, one on the front $V|_{t+\delta t} c^{i,\mathcal{GS}}$, where

$$V|_{t+\Delta t} \stackrel{\text{def}}{=} -\left(\frac{1-\Lambda}{4h^2}(D(x+h)+D(x-h))|_{t+\Delta t}\right) - \frac{1}{\Delta t} - \tau,$$

one ahead of the front

$$B^{(1)}|_{t+\Delta t} \stackrel{\text{def}}{=} \frac{1-\Lambda}{4h^2}(D(x+h)c^{i-1,\mathrm{SOR}}(x+2h))|_{t+\Delta t},$$

one behind the front

$$B^{(2)}|_{t+\Delta t} \stackrel{\text{def}}{=} \frac{1-\Lambda}{4h^2}(D(x-h)c^{i,\mathrm{SOR}}(x-2h))|_{t+\Delta t},$$

and one evaluated at the previous time t $Q|_t \stackrel{\text{def}}{=} \Lambda\lambda(c)|_t + c(x)/\Delta t|_t$. The Gauss–Seidel solution is

$$(B^{(1)} + B^{(2)})|_{t+\Delta t} + V|_{t+\Delta t} c^{i,GS}|_{t+\Delta t} + Q|_t = 0,$$

which leads to

$$c^{i,GS}|_{t+\Delta t} = -\frac{(B^{(1)} + B^{(2)})|_{t+\Delta t} + Q|_t}{V|_{t+\Delta t}}, \tag{10}$$

with the corresponding SOR acceleration being

$$c^{i,SOR}|_{t+\Delta t} = (1-\omega)c^{i-1,SOR}|_{t+\Delta t} + \omega c^{i,\mathcal{GS}}|_{t+\Delta t}. \tag{11}$$

This approach is standard (see for example [2,3] for details). The parameter $1 \leqslant \omega \leqslant 2$ is a "free" relaxation parameter which reduces the spectral radius of eigenvalues of the iteration matrix. For lack of any better value, we made the specific choice of $\omega = 1.5$ in the numerical experiments. The iterations were carried out until

$$\frac{\sum_{i=1}^{N} |c^{i+1} - c^i|}{\sum_{i=1}^{N} |c^{i+1}|} \leqslant \mathrm{tol} = 0.0000001$$

at each time step.

4.3. Criteria for crack front advancement

In the numerical simulations, we employ a simple criteria whereby when the average concentration in the process zone ligament ahead of the crack attains a critical value, which is scaled by a measure of the stress, the front is advanced. In order to motivate the stress dependent scaling, we employ an approach of "critical" concentration dependent stress intensity factors. Such ideas are somewhat standard in the application of fracture mechanics concepts to stress corrosion cracking, for example see works dating back at least to Brown [8]. We first consider a concentration dependent threshold stress intensity factor $K_{\mathrm{I}}^* \stackrel{\text{def}}{=} K_{\mathrm{I}}^*(c, K_{\mathrm{I}})$, which is an increasing function of concentration. We employ an evolution law of the form $\mathrm{d}K_{\mathrm{I}}^*/\mathrm{d}\bar{c} = AK_{\mathrm{I}}^*$, $K_{\mathrm{I}}^*(\bar{c} = 0) = K_{\mathrm{I}}$, where

$$\bar{c} = \langle c(x) \rangle_{r_p} \stackrel{\text{def}}{=} \frac{1}{r_p} \int_{r_p} c(x)\,\mathrm{d}x.$$

When the concentration is sufficiently high, and thus the concentration dependent stress intensity factor equals or exceeds a critical value, $K_{\mathrm{I}}^* \geqslant K_{\mathrm{I}}^{\mathrm{crit}}$, then subcritical fracture is said to occur. The solution to the evolution law is simply $K_{\mathrm{I}}^* = K_{\mathrm{I}} \mathrm{e}^{A\bar{c}}$, which leads to a simple definition for the critical hydrogen concentration in the process zone,

$$\bar{c}_{\mathrm{crit}} = \frac{1}{A} \ln\left(\frac{K_{\mathrm{I}}^{\mathrm{crit}}}{K_{\mathrm{I}}}\right).$$

When $\langle c(x) \rangle_{r_p} \geqslant \bar{c}_{\mathrm{crit}}$, or equivalently $K_{\mathrm{I}}^* \geqslant K_{\mathrm{I}}^{\mathrm{crit}}$, then the crack front is advanced. The critical

values are calibrated, later in the numerical experiments, by matching laboratory data on overall crack front velocity rates.

The overall advancing crack front algorithm is ($K_{\mathrm{I}} = \text{constant}$) [1]

$$
\begin{aligned}
&\text{Compute process zone size : } r_p = \frac{(K_{\mathrm{I}})^2}{2\pi \mathscr{Y}^2}(1-2\nu)^2 \\
&(\bigstar)\ \text{At a given time step } t \\
&\text{Compute the pressure field :} \\
&\quad P^{(t+\Delta t)}(x) = -\frac{2(1+\nu)}{3\mathscr{Y}}\frac{K_{\mathrm{I}}}{\sqrt{2\pi r_p}} \quad \forall x \text{ in process zone} \\
&\quad P^{(t+\Delta t)}(x) = -\frac{2(1+\nu)}{3\mathscr{Y}}\frac{K_{\mathrm{I}}}{\sqrt{2\pi x}} \\
&\qquad \forall x \text{ beyond process zone} \\
&\text{Compute transient concentration :} \\
&\quad \text{Starting distribution : } c^{(t+\Delta t)}(x) = c^{(t)}(x), \\
&\qquad \forall x \in (0, L) \\
&\quad \text{When } \langle c^{(t+\Delta t)} \rangle_{r_p} \geqslant \frac{1}{A}\ln\left(\frac{K_{\mathrm{I}}^{\mathrm{crit}}}{K_{\mathrm{I}}}\right) \\
&\qquad \text{advance front by } \Delta a^{(t+\Delta t)} = r_p \\
&c^{(t+\Delta t)}(x) = c_s = 1 \quad \forall x \text{ behind the advanced front} \\
&\text{Return to } (\bigstar) \text{ with updated values } (t = t + \Delta t).
\end{aligned}
\tag{12}
$$

Remark. The somewhat phenomenological material constant, A, is a result of the smaller scale mechanisms within the process zone, such as hydride formation, addressed in the works cited earlier.

5. Numerical experiments

The total grain boundary ligament ahead of the crack (Fig. 2), is chosen to be three times the length of a flattened grain from the mentioned laboratory experiments: $L = 3 \times 1100$ μm, $c(x = 0, t) = c_s = 1, c(x = L, t) = 0$. In the simulations, 3300 spatial (one node per micron) and 1000 temporal discretization nodes were used. This degree of discretization insured no changes in the solution for further numerical refinements for all the simulations in this work. The total computing time for a complete test run took a few seconds on a standard IBM RISC 6000 workstation. The material values used are taken from experiments in Zohdi and Meletis [35] for AL–2.2Li–2.9Cu–0.12Zr aluminum–lithium alloy in the T8 condition. The values are as follows: $\nu = 0.295$, $\mathscr{Y} = 307$ (MPa), $K_{\mathrm{I}} = 8.62$ MPa $\sqrt{\mathrm{m}}$. The selected mechanical parameters led to a computed process zone size of $r_p = 21$ μm, whereas the experimental values were approximately between 20 and 30 μm. The computed value for the crack tip radius was $\rho = 5.3$ μm. We defined a critical value for the pressure dependency parameter (η), which would force $U = U_0 + \widetilde{U}(P) = 0$ at the process zone boundary, $\eta^* \stackrel{\mathrm{def}}{=} -U_0/P(r_p)$. The experimental value of $U_0 = 7000$ (Nm/mol) for the activation energy was used. For the selected material values, $\eta^* = 1.059 \times 10^{-5}$ m^3/mol. The values of η were normalized by $\eta = \gamma\eta^*$, $0 \leqslant \gamma < 1$. As mentioned, the observed overall velocity measured from one hour's time was approximately 5×10^{-8} m/s, which leads to a front position of 3600 s $\times\ 5 \times 10^{-8}$ m/s $= 0.00018$ m after 1 h. Accordingly, for the numerical experiments we constructed the following parameter identification cost function

$$
\Pi \stackrel{\mathrm{def}}{=} \frac{|0.00018 - x_{\mathrm{f}}^{\mathrm{num}}(K_{\mathrm{I}}, A, \gamma, K_{\mathrm{I}}^{\mathrm{crit}})|}{0.00018}, \tag{13}
$$

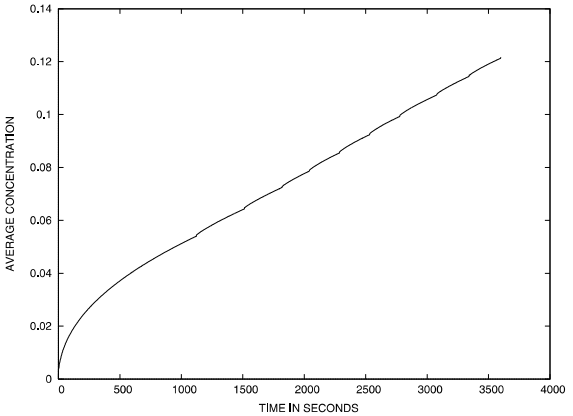

Fig. 4. $K_{\mathrm{I}} = 8.6$ MPa $\sqrt{\mathrm{m}}$, $\eta = 0.3\eta^*$ and $A = 0.1535$. The average concentration in the entire grain boundary.

[1] The stress intensity factor $K_{\mathrm{I}} = \sigma\sqrt{\pi a}$ is held constant by adjusting the remote stress (σ) due to the growing crack length (a).

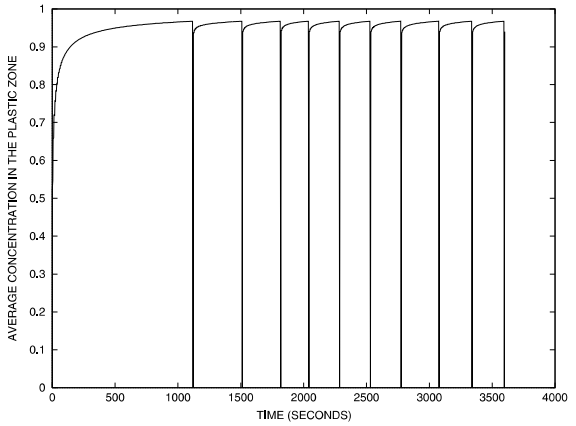

Fig. 5. $K_{\mathrm{I}} = 8.6$ MPa $\sqrt{\mathrm{m}}$, $\eta = 0.3\eta^{*}$ and $A = 0.1535$. The average concentration in the propagating front's current (continuously reformed) process zone.

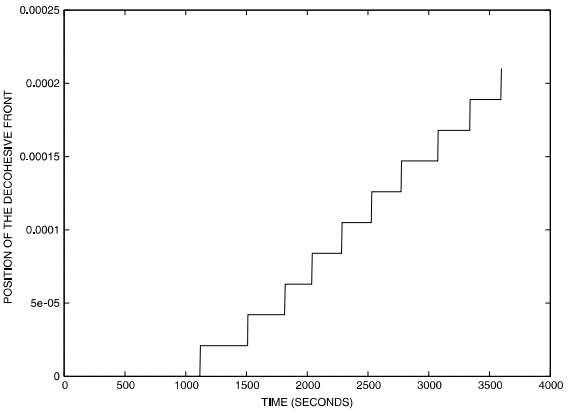

Fig. 6. $K_{\mathrm{I}} = 8.6$ MPa $\sqrt{\mathrm{m}}$, $\eta = 0.3\eta^{*}$ and $A = 0.1535$. The position of the moving front. Distributions at $(T = 3600)$, $t = 0.2T = 720\mathrm{s}$, $t = 0.4T = 1440\mathrm{s}$, $t = 0.6T = 2160\mathrm{s}$, $t = 0.8T = 2880\mathrm{s}$, $t = 1.0T = 3600\mathrm{s}$.

where $x_{\mathrm{f}}^{\mathrm{num}}(K_{\mathrm{I}}, A, \gamma, K_{\mathrm{I}}^{\mathrm{crit}})$ is the numerically computed front position for the given set of parameters. For the diffusivity, an experimental value of $D_0 = 2.2 \times 10^{-10}$ (m/s^2) was used. In order to narrow down the parameter studies, we set $K_{\mathrm{I}}^{\mathrm{crit}} = 10.0$ MPa $\sqrt{\mathrm{m}}$, which is slightly greater than the concentration-free load value of $K_{\mathrm{I}} = 8.62$ MPa $\sqrt{\mathrm{m}}$ used in the laboratory experiments. Consistent with laboratory experiments, in the first set of numerical experiments, for each individual time varying test, $K_{\mathrm{I}} = 8.62$ MPa $\sqrt{\mathrm{m}}$ was fixed. We performed studies varying $0 \leqslant \gamma = \eta/\eta^{*} \leqslant 1$, and allowing $A \geqslant 0$. The optimal parameter set (which minimized Π in Eq. (13)) was found to be approximately $(\gamma, A) = (0.3, 0.1535)$. The value of $A = 0.1535$, along with the stress intensity factors, leads to the following critical value for hydrogen, $\bar{c}_{\mathrm{crit}} = 0.9825$. The front propagation corresponding to this optimal set is shown in Figs. 4–7 for the optimal (γ, A) parameter set, with fixed $K_{\mathrm{I}} = 8.6$ MPa $\sqrt{\mathrm{m}}$. The averages in the entire original grain boundary length (fractured and still intact regions)

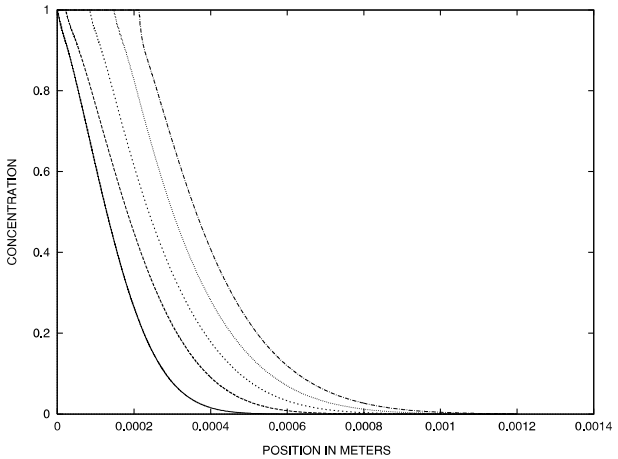

Fig. 7. $K_{\mathrm{I}} = 8.6$ MPa $\sqrt{\mathrm{m}}$, $\eta = 0.3\eta^{*}$ and $A = 0.1535$. Distributions of hydrogen in the intergranular zone. Distributions at $(T = 3600)$, $t = 0.2T = 720\mathrm{s}$, $t = 0.4T = 1440\mathrm{s}$, $t = 0.6T = 2160\mathrm{s}$, $t = 0.8T = 2880\mathrm{s}$, $t = 1.0T = 3600\mathrm{s}$.

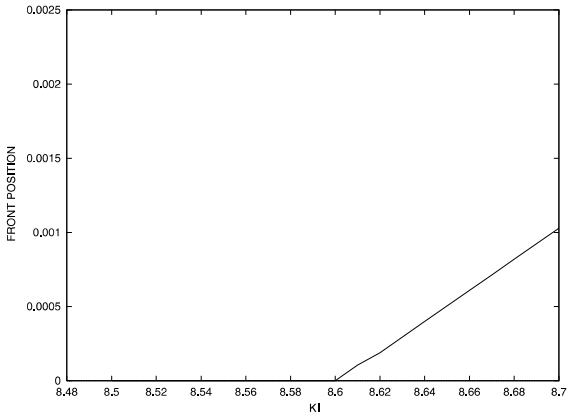

Fig. 8. The dependency on crack front position (after one hour) with variation of K_{I} for $(\gamma, A) = (0.3, 0.1535)$ and $\tau = 0.0$.

are shown in Fig 4. The curves contain small "ripples", stemming from the jump increase in the average concentration after each process zone ligament fracture. Correspondingly, after each ligament fracture there is a jump decrease in the concentration in the *newly* formed process zone. Since all of the highly hydrogen saturated material was fractured away, a period of time (an "incubation time") is required to build up the hydrogen to sufficiently critical levels in each new process zone (the dips in Fig. 5). The slightly different amounts of time to individual fracture are due to the residual, transient, amounts of hydrogen in the elastic zone which remain after the previous front advance (Figs. 6 and 7). These residual amounts lead to variations in the time to buildup a critical amount of hydrogen from jump to jump. In a further set of numerical experiments, the dependence of final front position on K_{I} (after 1 h), for the optimal set of (γ, A), was computed (Figs. 8 and 9). Themodel predicts monotonically linear growth with increasing K_{I}.

6. Concluding remarks

For many types of materials, the reactions with hydrogen can be autocatalytic, i.e. more hydrogen is produced as the reactions take place. This will lead to a higher buildup of hydrogen, and consequently faster intergranular cracking. However, in other cases, the hydrogen becomes neutralized after reaction, i.e. the hydrogen is consumed, thus leading to lower buildup in the process zone, and thus lower intergranular crack propagation rates. A classical *stoichiometrically inexact* approximation is to assume that the diffusing species reacts (is created or destroyed) in a manner such that the rate of production of the reactant (s) is directly proportional to the concentration of the diffusing species itself, $\dot{s} = \tau c$ [9]. Performing a mass balance leads to $\dot{c} = \nabla \cdot (\mathbb{D} \cdot \nabla c) - \tau c$, where when $\tau > 0$, the diffusing species is destroyed as it reacts, while $\tau < 0$ means that the diffusing species is created as it reacts, i.e. an autocatalytic or "chain" reaction

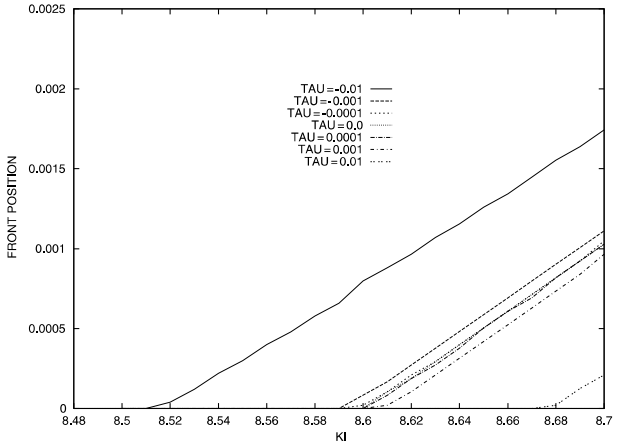

Fig. 9. The effect of variation of the reaction (τ) in the mass balance.

occurs. To illustrate the effects of reaction term, we fixed all material parameters, and varied τ. During each test, the reaction term was fixed to be a constant in the process zone, and zero outside of the process zone. Figs. 8 and 9 depict the results. As one would expect, the rates of crack propagation monotonically increase with increased autocatalyzation. Essentially the curves shift up or down, in a parallel manner, depending on degree of autocatalyzation. The precise calibration of τ with laboratory tests is a topic of ongoing research of the author.

Finally, to a structural analyst, the estimation of macroscopic degradation rates from intergranular crack propagation rates is of fundamental interest. However, it is clear that analyses, such as the one presented here, are, to an extent, phenomenological. To overcome this, more detailed analyses, such as those mentioned at the outset of this work dealing with hydride inclusion formation and those addressing the effect of hydrogen on the stress field themselves *during the diffusion process*, are necessary to determine the dominant micromechanisms in the process zone which control the pausing of the crack front leading to an *incubation time*.

References

[1] E.C. Aifantis, A new interpretation of diffusion in regions with high diffusivity paths: a continuum approach, Acta Metall. 27 (1979) 683–691.

[2] W.F. Ames, Numerical Methods for Partial Differential Equations, second ed., Academic Press, New York, 1977.

[3] O. Axelsson, Iterative Solution Methods, Cambridge University Press, Cambridge, MA, 1994.

[4] H.K. Birnbaum, Environment-sensitive fracture of engineering materials, in: Z.A. Foroulis (Ed.), TMS-AIME, 1979, p. 326.

[5] H.K. Birnbaum, Hydrogen related second phase embrittlement of solids, in: R. Gibala, R.F. Hehemann (Eds.), Hydrogen Embrittlement and Stress Corrosion Cracking. Proceeding of a Troiano Festchrift Symposium, Case Western Reserve University, 1–3 June 1980, ASM, OH, pp. 153–177.

[6] H.K. Birnbaum, Mechanisms of hydrogen related fracture of metals, in: N.R. Moody, A.W. Thompson (Eds.), Hydrogen effects on material behavior. Proceedings of the Fourth International Conference on the Effects of Hydrogen on the Behavior of Materials, The Minerals, Metals and Materials Society, Moran, Wyoming, 12–15 September 1989, pp. 639–690.

[7] H.K. Birnbaum, P. Sofronis, Hydrogen-enhanced localized plasticity—a mechanism for hydrogen related fracture, Mat. Sci. Eng. A 176 (1994) 191–202.

[8] B.F. Brown, The application of fracture mechanics concepts to scc, Metals Mat. Met. Rev. 2 (13) (1968) 171–183.

[9] J. Crank, The Mathematics of Diffusion, second ed., Oxford Science Publications, 1975.

[10] P. Doig, T. Jones, A model for the initiation of hydrogen embrittlement cracking at notches in gaseous hydrogen environments, Metall. Trans. 18A (1977) 1993–1998.

[11] R. Dutton, K. Nuttall, M.P. Puls, L.A. Simpson, Mechanisms of hydrogen induced delayed cracking in hydride forming materials, Met. Trans. 8A (1977) 1553–1562.

[12] F. Ellyin, J. Wu, Effect of hydride precipitation on the elastoplastic stress field near a crack tip, Acta. Metall. 42 (1994) 2709–2717.

[13] C.P. Flynn, Point Defects and Diffusion, Clarendon Press, Oxford, 1972.

[14] M.G. Fontana, Corrosion Engineering, third ed., McGraw-Hill, Maidenherd, 1986.

[15] Metals Handbook, Failure Analysis and Prevention, Vol. 8, The American Society for Metals, 1975.

[16] B.W. Leitch, M.P. Puls, Finite element calculations of the accomodation energy of a misfitting precipitate in an elastic–plastic matrix, Met. Trans. 23A (1992) 797–806.

[17] H.W. Liu, Stress corrosion cracking and the interaction between crack-tip stress-field and solute atoms, J. Basic Eng. ASME. 92 (1970) 633–638.

[18] J. Lufrano, P. Sofronis, Numerical analysis of the interaction of solute hydrogen atoms with the stress field of a crack, Intl. J. Solids Struct. 33 (12) (1996) 1709–1723.

[19] J. Lufrano, P. Sofronis, H.K. Birnbaum, Modeling of hydrogen transport and elastically accommodated hydride formation near a crack tip, J. Mech. Phys. Solids. 44 (1996) 179–205.

[20] J. Lufrano, P. Sofronis, H.K. Birnbaum, Elastoplastically accommodated hydride formation and embrittlement, J. Mech. Phys. Solids 46 (9) (1998) 1497–1520.

[21] S.M. Schlögel, E. Van der Giessen, Hydrogen attack inawelded reactor, J. Phys. IV France 9 (1999) 137–146.

[22] S.M. Schlögel, Y. Van Leeuwen, E. Van der Giessen, On methane generation and decarburization in low alloy Cr–Mo steels during hydrogen attack, A 31 (2000) 125–137.

[23] P. Sofronis, R.M. McMeeking, Numerical analysis of hydrogen transport near a blunting cracktip, J. Mech. Phys. Solids. 37 (1989) 317–350.

[24] D.J. Unger, W.W. Gerberich, D.C. Aifantis, Further remarks on the implications of steady-state stress-assisted diffusion on environmental cracking, Scripta Metall. 16 (1982) 1059–1064.

[25] D.J. Unger, D.C. Aifantis, On the theory of stress-assisted diffusion, II. Acta Mech. 47 (1983) 117–151.

[26] D. Unger, A mathematical analysis of impending hydrogen assisted crack propagation, Eng. Fract. Mech. 34 (1989) 657–667.

[27] D. Unger, A mathematical analysis of impending hydrogen assisted crack propagation, Eng. Fract. Mech. 34 (1989) 657–667.

[28] M.W.D. Van der Burg, E. Van der Giessen, R.C. Brouwer, Investigation of hydrogen attack in 2.25Cr–1Mo steels with a high-triaxiality void growth model, Acta Mater. 44 (2) (1996) 505–518.
[29] M.W.D. Van der Burg, E. Van der Giessen, A continuum damage relation for hydrogen attack cavitation, Acta. Mater. 45 (7) (1997) 3047–3057.
[30] M.W.D. Van der Burg, E. Van der Giessen, V. Tvergaard, A continuum damage analysis of hydrogen attack in 2.25Cr–1 Mo pressure vessel, Mat. Sci. Eng. A 241 (1998) 1–13.
[31] H.P. Van Leeuwen, A quantitative model of hydrogen induced grain boundary cracking, Corrosion 29 (1973) 197–204.
[32] H.P. Van Leeuwen, The kinetics of hydrogen embrittlement: a quantitative diffusion model, Eng. Fract. Mech. 6 (1974) 141–161.
[33] H.P. Van Leeuwen, Plateau velocity of SCC in high strength steel—a quantitative treatment, J. Corrosion. NACE. 31 (2) (1975) 42–50.
[34] D.G. Westlake, A generalized model for hydrogen embrittlement, Trans. ASM. 62 (1969) 1000–1006.
[35] T.I. Zohdi, E.I. Meletis, On the intergranular hydrogen embrittlement mechanism of Al–Li alloys, Scripta Metall. 26 (1992) 1615–1620.
[36] T.I. Zohdi, Some remarks on hydrogen trapping, Intl. J. Fract. 106 (2) (2000) L9–L14.